Simple modeling of single-mode inhomogeneously broadened laser dynamics

B. Meziane* and H. Ladjouze*
Laboratoire d'Optronique, Ecole Nationale Supérieure des Sciences Appliquées et des Technologie, 6 Rue de Kérampont, Boîte Postale 447, 22305 Lannion CEDEX, France
(Received 5 February 1991; revised manuscript received 19 June 1991)

This paper presents a review of a few low-dimensional models which describe some of the dynamical properties of the single-mode inhomogeneously broadened, unidirectional ring laser, and points out the limits of their validity in comparison to the integro-differential equations from which they are derived. A 6D model that seems to circumvent the weaknesses of the other models is also proposed. A numerical analysis with parameter values that correspond to two-laser systems shows a good description of most of the qualitative dynamical aspects exhibited by these systems. The simplicity of our model will allow for a deep numerical investigation, and will yield a better insight into the physical mechanisms connected with single-mode inhomogeneously broadened laser dynamics.

PACS number(s): 42.60.Mi, 42.55.−f, 42.50.Lc, 42.50.Fx

I. INTRODUCTION

Since the experimental observation by Casperson and Yariv of low-excitation trains of pulses in the He-Xe laser [1], the modeling of the dynamical properties of single-mode inhomogeneously broadened (SMIB) lasers has, especially for the past few years, been the focus of multiple papers from various authors [2–14]. In particular, considerable interest followed the emergence of an exciting branch of physics dealing with the analysis of nonlinear phenomena, for which the ever growing capabilities of computers have transformed analytically intractable dynamical problems into easier problems of merely finding more or less exotic temporal solutions after entering some control parameters of the system under study into the computer. These numerical facilities have given a real burst to the resurgence of laser theory in connection to its dynamical aspects.

Even though unstable solutions in laser systems were indeed known to exist before the construction of the laser itself [15], and erratic numerical solutions were obtained without a noise source [16], one had to wait for the Haken's finding [17] of the equivalence between the equations describing the dynamics of a single-mode homogeneously broadened (SMHB) laser and the Lorenz model of turbulence in fluids [18], for a correct understanding of the obtained results. It then became clear that the set of dynamical equations describing the behavior of a laser was merely a member of a large family of nonlinearly described phenomena. These phenomena are not limited to physics, but extend to hydrodynamics, economics, chemical reactions, and biology, to name just a few (for a comprehensive understanding of these phenomena see Ref. [33]). The link between the dynamics pertaining to such various fields is an exciting branch of science called "deterministic chaos" in which a number of universal laws have become tools in the study of nonlinear problems [19–21,33]. On the experimental side of laser systems, however, apart from the Casperson instability, whose theoretical analysis is fully contained, both qualitatively and quantitatively, in the integro-differential (so-called Maxwell-Bloch) equations, some uncertainty continues to surround the interface between experimental data and the corresponding theoretical models. In the case of the single-mode homogeneously broadened laser, for example, the necessary excitation level (second laser threshold), which is nine times higher than the threshold for laser action, is a nearly unattainable limitation for the observation of Lorenz chaos in such a system. Active experimental research still surrounds this question and successful attempts may be expected in the near future.

Investigations pertaining to the SMIB laser have, however, followed quite a different route. Self-pulsing in a high-gain He-Xe laser has been observed by Casperson and Yariv [1], and this quite uncommon type of behavior was attributed to transient relaxation oscillations of the system [22]. It took Casperson quite a few years to derive an acceptable model which gives an exact account of the observed undamped trains of pulses [23,24]. The difficulty was mainly due to the fact that the theory, based on self-consistency assumptions that was derived by Lamb to describe laser properties, had long been recognized as giving a fairly good account of many of the observable phenomena in laser systems (mode pulling, mode pushing, saturation effects, Lamb dip, etc.) [26,27]. Lamb's theory, however, has its roots based in a self-consistency analysis in which the polarization of the medium is supposed to respond instantaneously to the electric field inside the cavity. In other words, the basis of Lamb's theory is an adiabatic elimination of the medium's polarization, which is a fast-relaxing variable controlled by the slow-relaxing optical field and population inversion. Even though in a large number of laser systems the polarization, indeed follows the electric field adiabatically, yielding dynamical behavior described in terms of the well-known "rate equations," this is not true for a certain class of systems, to which the He-Xe laser studied by Casperson and Yariv belongs.

During the past few years a number of authors have paid quite a lot of attention to the theoretical as well as to

the experimental aspects of SMIB lasers. The dynamical properties of such a system have been the subject of various conclusive papers [2–14,25]. Two aspects of the theory may be clearly distinguished: first, a numerical analysis, which is a straightforward task, and second an analytical aspect which requires relatively complicated algebra for which the physical insight is not always clear, because of a polarization integral that renders the system of infinitely high dimension, especially when compared to the case of a SMHB laser, for which both aspects are straightforward, and a simple analytical expression is derived for the position of the second laser threshold (instability threshold).

Some simple (low-dimensional) models have also been constructed to give some account of the dynamics inherent in the infinite-dimensional (integro-differential Maxwell-Bloch equations) system [28–31]. Each of these models is, however, constructed only to describe a particular situation out of the wealth of dynamical properties of the "Maxwell-Bloch" equations (self-pulsing, periodic oscillations, chaos, etc.). None of the models proposed so far contains even qualitatively, the different physical situations inherent in the exact integro-differential set of equations.

The purpose of this paper is twofold: First, it is meant to give a quick review of some of the known simple models along with some criticisms and limitations in comparison to the Maxwell-Bloch equations; second, we propose a model with six equations which seems to match, at least qualitatively, most of the dynamics of a SMIB laser.

Section II is devoted to a review of the Maxwell-Bloch equations with some hints pertaining to the numerical analysis, as well as to a remainder of the dynamic behavior of the system according to the values of the control parameters (excitation parameter C, cavity relaxation rate k, etc.). Section III concerns a rapid review of (a) the Graham and Cho model [28], (b) our four-dimensional (4D) model, which describes the "Casperson instability" [29,30], and (c) the Idiatulin and Uspenskii model [31]. In Sec. IV another simple model is constructed for which a one-to-one analogy with the Maxwell-Bloch equations is undertaken for a large range of its control parameters. We will take advantage of the simplicity of our model to carry out a deeper numerical investigation, and attempt to identify the physical mechanisms responsible for some of the dynamical properties of SMIB lasers. Some attention will also be given to the rate-equations approximation, and the adiabatic-field approximation in order to gain some more physical insight. Section IV concludes with some focus on the effect of an additional detuning parameter on the general dynamical features of the system. Finally in Sec. V we give some conclusions and delimit the extent of validity of the simple modeling of SMIB laser dynamics.

II. DESCRIPTION OF THE MAXWELL-BLOCH EQUATIONS

The SMIB, unidirectional ring laser is modeled with the help of an interaction picture between a collection of two-level atoms and the resonant optical field, which in turn satisfies the Maxwell propagation equation. Such a modeling yields equations of motion for the field and atomic variables which, in the slowly-varying-envelope approximation, and in the absence of detuning, take the form

$$\frac{d[E(t)]}{dt}=-k\left[(E(t)+2C\int_{-\infty}^{+\infty}dw\,g(w)p(w,t)\right], \quad (1a)$$

$$\frac{d[p(w,t)]}{dt}=-(1+iw)p(w,t)+E(t)d(w,t), \quad (1b)$$

$$\frac{d[d(w,t)]}{dt}=-\gamma\{d(w,t)+1+1/2[E(t)p^*(w,t)+E^*(t)p(w,t)]\}, \quad (1c)$$

and are usually referred to as the Maxwell-Bloch equations.

In our notation $E(t)$ is the slowly varying output-field amplitude scaled to the square root of the saturation intensity, $p(w,t)$ and $d(w,t)$ denote the polarization and population difference, respectively, of an arbitrary atomic homogeneous packet positioned w away from the line center in the spectral profile, k and γ are, respectively, the cavity decay rate and the relaxation rate of the population difference, both scaled to the polarization relaxation rate, $g(w)$ is the atomic spectral distribution, C is the excitation parameter, and t is a dimensionless variable representing the product of time and the polarization relaxation rate (for details see Refs. [7,8,29]).

Because of the polarization integral in Eq. (1a), set (1) is a dynamical system of infinite dimension. It is found that the continuous integral must be discretized into at least 100 atomic packets for a compromise between accuracy and speed of execution in the numerical simulations [8,24]. Some hints can save half the task if, for the gain profile of the active medium, we take a Gaussian distribution:

$$g(w)=(1/\sqrt{2\pi}\sigma_D)\exp(-w^2/2\sigma_D^2), \quad (2)$$

where σ_D is the half width, at half maximum, of the atomic spectral profile, also scaled to the polarization relaxation rate, and the atomic variables satisfy the conditions

$$d(-w,t)=d(w,t), \quad (3a)$$

$$p(-w,t)=p^*(w,t), \quad (3b)$$

and for central tuning the optical field can be taken to be real without loss of generality. With these symmetrical properties set (1) is transformed into another set which requires only 50 atomic components for the same compromise as above:

$$\frac{d[E(t)]}{dt} = -k\left[E(t)+2C\int_0^{+\infty} dw\, g(w)[p(w,t)+p^*(w,t)]\right], \tag{4a}$$

$$\frac{d[p(w,t)]}{dt} = -(1+iw)p(w,t)+E(t)d(w,t), \tag{4b}$$

$$\frac{d[d(w,t)]}{dt} = -\gamma\{d(w,t)+1+[\tfrac{1}{2}E(t)][p(w,t)+p^*(w,t)]\}. \tag{4c}$$

The dynamics inherent in set (1) has been the subject of an extensive literature. Depending on the numerical values of k, γ, and C, a wealth of dynamical properties is contained in these integro-differential equations in the bad-cavity case ($k>1+\gamma$). The temporal trace shows periodic oscillations, regular self-pulsing, erratic modulation as well as a period-doubling route to chaos, and intermittency.

Although the numerical analysis is a straightforward task which involves a standard fourth-order Runge-Kutta scheme for the differential equations along with a Simpson rule for the polarization integral, the relatively complicated algebra involved in the linear stability analysis, usually performed in order to extract the conditions under which the system becomes unstable (yielding especially the second laser threshold), hides much of the physical insight, especially when compared to the equations of a single-mode homogeneously broadened laser which have been shown to be equivalent to the Lorenz model of turbulence in fluids.

A number of low-dimensional models have been proposed as the Lorenz-like models of SMIB lasers. Even though the proposed models indeed show some of the qualitative features inherent in the integro-differential set (1) for some particular values of γ, k, and C, the wealth of dynamical properties of set (1) cannot be matched with any of these models in a large span of physical situations related to the values of the system parameters γ, k, and C.

III. SOME SIMPLE MODELS

A. Graham and Cho model

It was proposed by the above authors [28]. Its construction follows from the reduction of the integro-differential equations (1) to a set of four differential equations in which macroscopic variables of the medium (total polarization and total population inversion) are coupled to the field instead of microscopic ones (polarization and population inversion of groups of atoms). The procedure is based on the creation of new variables related to the polarization and to the population inversion of the medium, and an adjustable parameter carefully chosen so as to truncate the infinite hierarchy of coupled equations generated in this way. This procedure yields a set of four differential equations:

$$\frac{d[E(t)]}{dt} = -k[E(t)+2CP(t)], \tag{5a}$$

$$\frac{d[P(t)]}{dt} = -P(t)+E(t)D(t)+s^2S(t), \tag{5b}$$

$$\frac{d[D(t)]}{dt} = -\gamma[E(t)P(t)+D(t)+1], \tag{5c}$$

$$\frac{d[S(t)]}{dt} = [-S(t)+P(t)], \tag{5d}$$

where macroscopic variables

$$P(t) = \int_{-\infty}^{+\infty} dw\, g(w)p(w,t),$$
$$D(t) = \int_{-\infty}^{+\infty} dw\, g(w)d(w,t), \tag{6}$$

have been introduced, and the new variable $S(t)$ is defined by

$$s^2S(t) = \int_{-\infty}^{+\infty} dw\, w^2 g(w)p(w,t), \tag{7}$$

and s^2 is chosen in the form

$$s^2 = \int_{-\infty}^{+\infty} dw\, w^2 g(w)p_0(w)\int_{-\infty}^{+\infty} dw\, g(w)p_0(w) \tag{8}$$

so as to close the generated infinite hierarchy of coupled equations. $p_0(w)$ represents the value of the atomic polarization at steady state [when all the derivatives in Eqs. (1) are set equal to zero].

A straightforward linear stability analysis of set (5) yields a much lower second laser threshold than the second threshold of the SMHB lasers for the same parameter values. This is the central analytical result of this model.

The numerical analysis shows the appearance of a limit cycle immediately above the second laser threshold, which bifurcates to a strange attractor for larger values of the excitation parameter C. This dynamical regime is also exhibited by set (1) in the bad-cavity and radiative limit ($\gamma=1$) case. However, for low values of γ, set (1) exhibits regular and irregular self-pulsing (referred to as the Casperson instability), while set (5) fails to describe this self-pulsing behavior, as shown in Ref. [29]. The validity of set (5), as compared to Eqs. (1), is limited to γ values close to unity.

B. 4D self-pulsing model

The construction of this model is deeply rooted in the above Graham and Cho model. It stems from a heuristic readjustment of the parameter s^2 in order to extend its validity to a larger region of the field intensity, yielding a better match with the Maxwell-Bloch equations in the conditions of self-pulsing, and allows for a better description of Casperson's experimental and numerical results [2,25].

A readjustment of s^2 that takes into account some physical processes in the laser medium has been chosen in the form [29]

$$s^2 \rightarrow s^2/[1+E(t)^2] \ . \tag{9}$$

With this expression for the parameter s^2 a new equation if obtained for the macroscopic polarization and the set of coupled equations (5) transforms into

$$\frac{d[E(t)]}{dt} = -k[E(t)+2CP(t)] \ , \tag{10a}$$

$$\frac{d[P(t)]}{dt} = -P(t)+E(t)D(t)+[s^2/(1+E^2)]S(t) \ , \tag{10b}$$

$$\frac{d[D(t)]}{dt} = -\gamma[E(t)P(t)+D(t)+1] \ , \tag{10c}$$

$$\frac{d[S(t)]}{dt} = -[S(t)+P(t)] \ . \tag{10d}$$

The numerical analysis of this set of equations for parameter values of γ and k corresponding to the He-Xe laser shows the presence of reproducible and regular low-excitation spontaneous pulsations with an increase of pulse repetition rate and amplitude with increasing C. Furthermore, it was shown that an adiabatic elimination of the field variable still retained the dynamical aspects of the 4D set 10, a feature which is in good agreement with Casperson's results, and also inherent in the integro-differential set 1 [25,29].

However, it is worthwhile to point out the limitations of this model. In cases where a self-pulsing in the form of regular pulse trains is present, the set of equations (10) is an adequate approximation of the Maxwell-Bloch equations. For parameter values of γ, k, and C for which Eqs. (1) develop periodic oscillations (for example, in the radiative limit $\gamma=1$), period-doubling bifurcations, erratic modulation, etc., the dynamics of set 10 deviates from the integro-differential equations.

Another readjustment of s^2 stemming from the same heuristic considerations has also been proposed [30]:

$$s^2 \rightarrow s^2 \exp[-E(t)^2] \ . \tag{11}$$

With this other form for s^2, a new set of equations is obtained from Eqs. (5) showing the same self-pulsing behavior as Eqs. (10). Furthermore, the period-doubling route to chaos contained in set (1) is retrieved. However, this new set is characterized by the same other limitations as set (10).

C. Idiatulin and Uspenskii model

This model was proposed by the above authors [31], who demonstrated theoretically that expanding the inhomogeneous medium to two groups of atoms, with different resonant frequencies, brought about qualitative changes as well as a significant reduction in the laser instability threshold. This model has recently received some new attention [32]. It seems to be well adapted for the explanation of the experimentally observed self-sustained oscillations in far-infrared lasers for which $\gamma=1$.

The equations of motion are straightforwardly derived from set 4 by replacing the polarization integral by the sum of two components situated at $-w$ and $+w$ in the spectral profile; in so doing the following equations are obtained:

$$\frac{d[E(t)]}{dt} = -k\{E(t)+2C[p(w,t)+p^*(w,t)]\} \ , \tag{12a}$$

$$\frac{d[p(w,t)]}{dt} = -(1+iw)p(w,t)+E(t)d(w,t) \ , \tag{12b}$$

$$\frac{d[d(w,t)]}{dt} = -\gamma\{d(w,t)+1 + \tfrac{1}{2}E(t)[p(w,t)+p^*(w,t)]\} \ . \tag{12c}$$

Idiatulin and Uspenskii did not characterize the dynamical properties of their model but limited their studies to linear stability analysis of the steady-state solutions for the purpose of finding the conditions of an instability emergence. Some results of a numerical analysis, in the bad-cavity case ($k=5$), and for γ in the vicinity of the radiative limit, have recently been published by Abraham *et al.* in the context of a theoretical link with the observations of undamped pulsations in a FIR laser [32]. This 4D model shows an intensity time trace in the form of regular oscillations for a low-excitation parameter, evolving towards an intermittent time dependence with an increase of the control parameter C.

However, as in the case of set (5), Eqs. (12) fail to describe the self-pulsing characteristics of set (1) for low values of γ.

The main conclusion here is that all the low-dimensional models proposed to date have a limited validity compared to the integro-differential equations from which they are derived. Either a given model describes the self-oscillation characteristics inherent in set (1) for values of γ close to the radiative limit, in which case the model is not adapted to describe the dynamics of the original set for low values of γ, or it does describe the self-pulsing nature but fails to describe the dynamics for $\gamma=1$.

It is also worthwhile mentioning the identity between the apparently different sets of Eqs. (5) and Eqs. (12). For the numerical value of s^2 chosen by Graham and Cho in their analysis the set of equations (5) corresponds exactly to set (12) in the case where $w=1$. The truncation proposed by Graham and Cho is merely equivalent to the Idiatulin and Uspenskii equations, at least in the 4D model, and for the chosen value of s^2. This explains the low-excitation limit cycles obtained in Ref. [28], which correspond to the self-oscillations of Ref. [32].

IV. CONSTRUCTION OF A 6D MODEL

The weaknesses of the preceding models can all be circumvented with the help of a 6D model constructed along the lines of the Idiatulin and Uspenskii model with additional central tuned atomic variables. In other words, it is enough to replace the polarization integral of Eqs. (1) with three atomic components at, respectively, $-w$, 0, and $+w$ in the spectral profile. The equations of motion are the set of equations (12) with two additional

equations for the polarization and population inversion of the central component. In real space the model is described with the following set:

$$\frac{d[E(t)]}{dt} = -k\{E(t)+2C[2p_r(t)+p_0(t)]\} , \tag{13a}$$

$$\frac{d[p_r(t)]}{dt} = -p_r + wp_i + E(t)D(t) , \tag{13b}$$

$$\frac{d[p_i(t)]}{dt} = -p_i - wp_r , \tag{13c}$$

$$\frac{d[D(t)]}{dt} = -\gamma[D(t)+1+E(t)p_r] , \tag{13d}$$

$$\frac{d[p_0(t)]}{dt} = -p_0 + E(t)D_0(t) , \tag{13e}$$

$$\frac{d[D_0(t)]}{dt} = -\gamma[D_0(t)+1+E(t)p_0(t)] , \tag{13f}$$

where p_r and p_i are the real and imaginary parts, respectively, of the polarization component $p(w,t)$, p_0 is the polarization central component.

At first sight there is no apparent reason why the addition of the last two equations to set (12) should result in a sensitive difference in behavior. However, as the numerical analysis reveals, the additional equations allow the system to contain most of the dominant properties exhibited by the integro-differential equations (1). It gives a fairly good account of the dynamics of set (1) in a much larger range of physical situations when we compare to the 4D models of Sec. III. Just as the Maxwell-Bloch equations do, our 6D model describes features such as (i) self-sustained periodic oscillations, (ii) erratic modulation of the field intensity, (iii) regular and irregular trains of pulses, (iv) period doubling bifurcations leading to chaos, and (v) intermittency.

It then seems that this model is able to solve the discrepancies shown by the models described in Secs. III A–III C, and is well adapted for the description of SMIB laser dynamics. In order to keep close contact with experimentally known results we have numerically solved Eqs. (13) with parameter values first corresponding to the FIR laser ($\gamma=1$), second to the case of the He-Xe laser ($\gamma=0.05$).

The first system is known to exhibit periodic oscillations in its output intensity for low-excitation parameter C as observed experimentally in Ref. [32], and the second example shows regular trains of pulses as first obtained by Casperson and Yariv, and subsequently thoroughly studied by Abraham *et al.* [3,5].

In order to allow for a first glance comparison with published data [8] of the numerical analysis of set (1), we have chosen to scan the excitation level in terms of the parameter X_s instead of C. The two parameters are indeed related through the state equation, derived from set (13) when all the derivatives are set equal to zero:

$$4C[1/(1+w^2+X_s^2)+0.5/(1+X_s^2)]=1 , \tag{14}$$

where X_s represents the square root of the field intensity at steady state.

Let us consider in detail the results of a few typical scans. In all the cases of the numerical analysis, we selected a bad-cavity configuration with a normalized cavity decay rate $k=5$. The γ values corresponding to the above-mentioned experiments are $\gamma=1$ (radiative limit) appropriate to the FIR laser, and $\gamma=0.05$ appropriate to the 3.51-μm He-Xe laser. Note that the positions of the atomic components $\pm w$ in the spectral profile are chosen according to the value of the inhomogeneous linewidth σ_D, in such a way that the relation

$$\int_0^w g(w)dw = \int_w^\infty g(w)dw \tag{15}$$

is satisfied. For simplicity we have set w, as given by the above relation, as equal to its closest integer: In the case of the He-Xe laser $\sigma_D \cong 5$ yields $w \cong 1$. For the second case, $w=2$ is taken from the literature [32] as the separation between two groups of atoms (which coexist in the FIR laser), and the central line.

Figures 1 and 2 show typical results obtained for the two chosen examples.

Among other scans, worth mentioning are the following facts.

In the case of $\gamma=1$, which corresponds to an equality between the rate of incoherent decay of the population inversion and the polarization decay rate, the following general pattern has emerged: over a certain range of the gain related parameter X_s, regular output oscillations are developed, then for larger gain values, it shows period-doubling bifurcations to chaos in a rather narrow window of the gain-parameter values. This fact is inherent in the integro-differential set (1) as shown in Ref. [8]. This type of behavior does not make any experimental sense in view of the extremely small window of period doubling. For slightly higher values of the gain parameter the developed pattern is suggestive of some kind of intermittency. The system remains in this intermittent type of evolution for a large range of the excitation parameter, and much beyond the excitation level of Fig. 2(f).

When the rate of incoherent decay of the population difference is much smaller than the polarization decay rate, the intensity output has the form of regular trains of pulses for some range of the excitation parameter. Upon increasing the gain parameter it develops a series of period-doubling bifurcations to chaos. The range of the excitation parameter values corresponding to these bifurcations is rather large when compared to the above case. This explains why such a route has been experimentally observed in He-Xe lasers for which the chosen values of the control parameters apply. Distinct period-doubling windows have been found, which are clearly distinguished in Figs. 1(a) and 1(d) for some distant values of the excitation parameter. Such double-pulse windows have been observed experimentally by Casperson [25]. These results convincingly show the correspondence of the Maxwell-Bloch equations and the set of equations (13).

Now that a clear analogy between the original integro-differential equations and the set of equations (13) has been demonstrated, we shall take advantage of the simplicity of our 6D model and carry out a deeper investigation

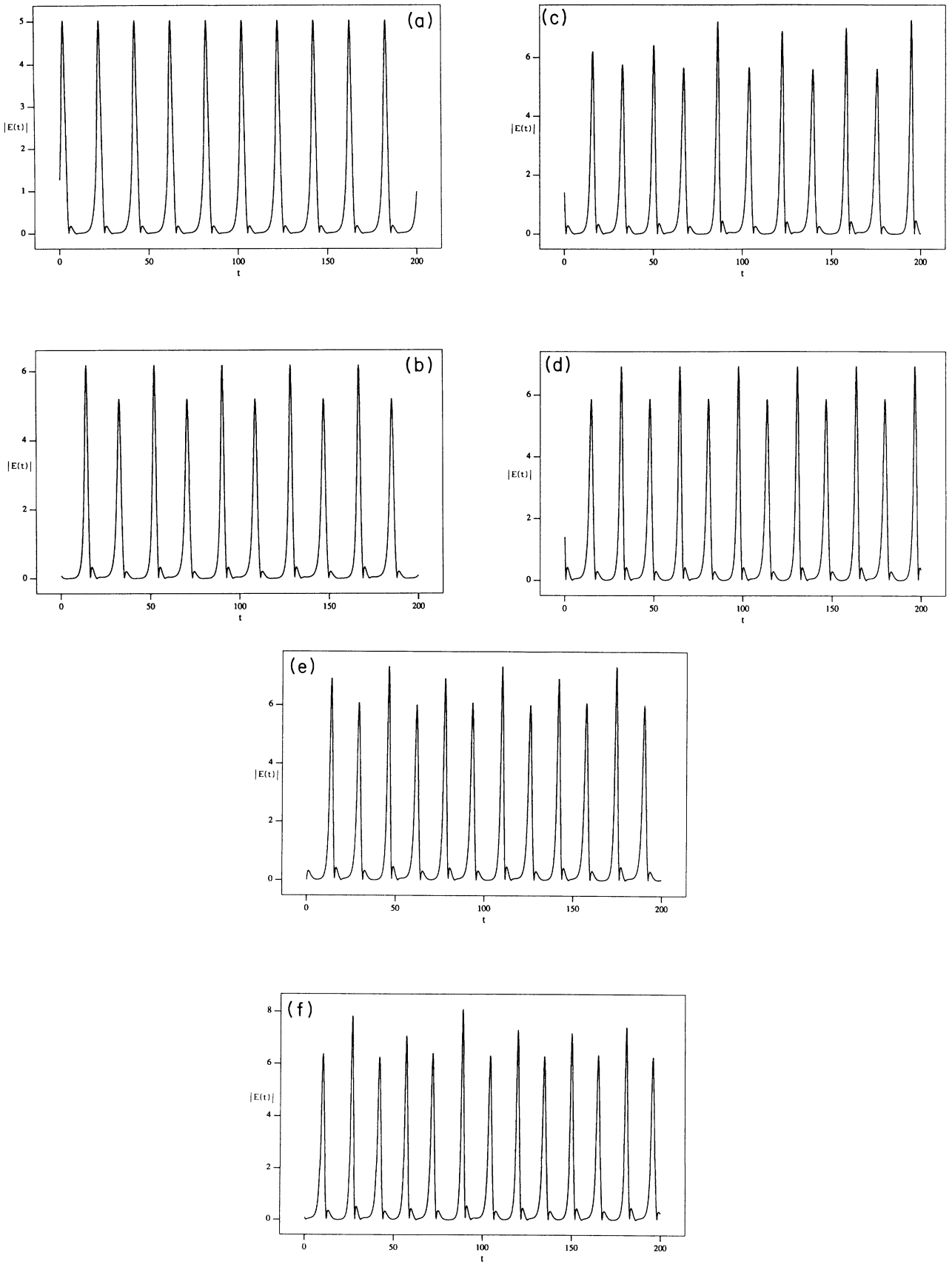

FIG. 1. Nontransient trains of pulses for $k=5$, $\gamma=0.05$, $w=1$, and increasing values of X_s; (a) regular pulses for $X_s=1.6$, (b) development of a period-doubling pattern for $X_s=1.75$, and (c) irregular (chaotic) train of pulses for $X_s=1.9$.

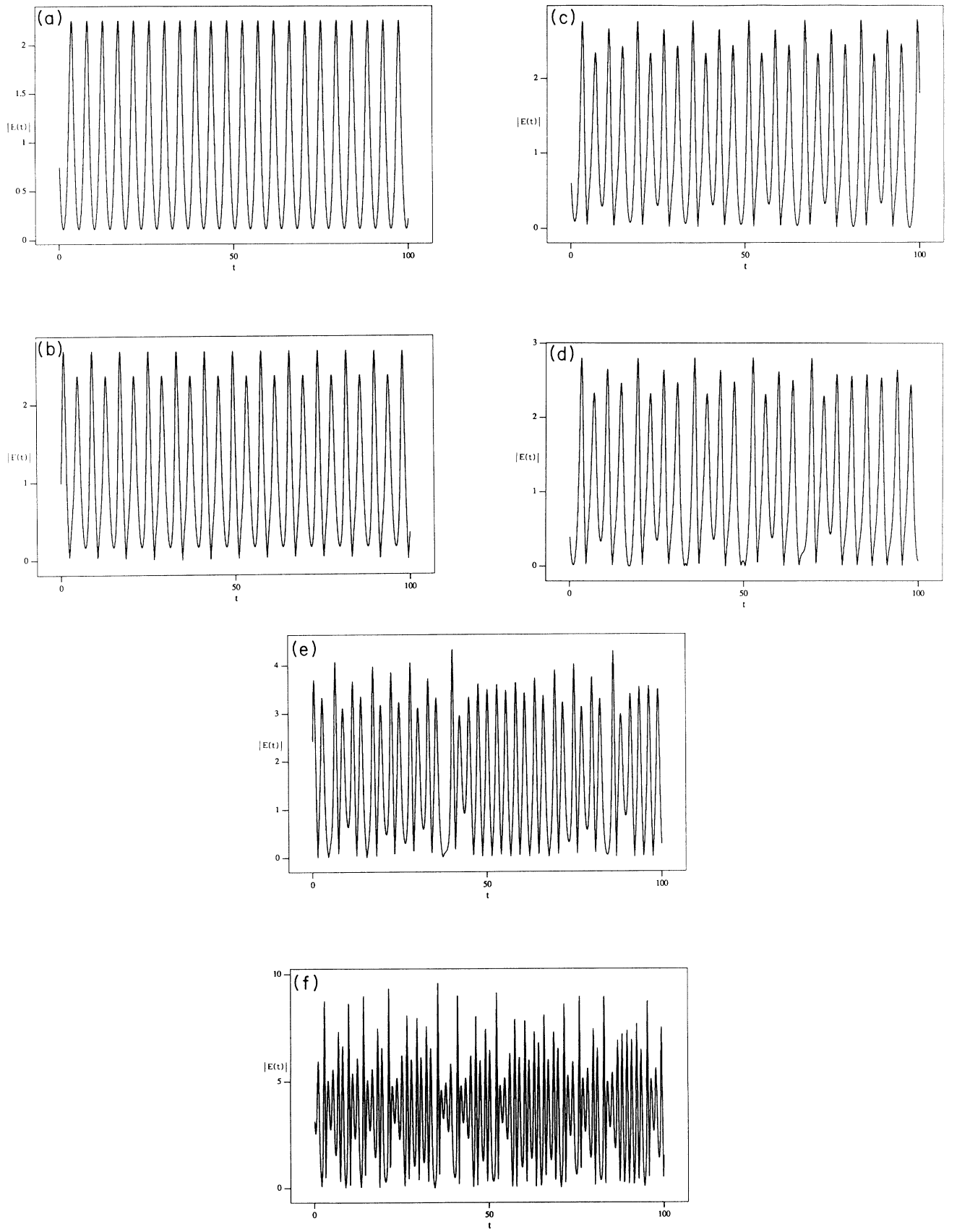

FIG. 2. Time dependence of $[E(t)]$ for $k=5$, $\gamma=1$, and $w=2$ (a) periodic oscillations for $X_s=1.3$, (b) period-doubled oscillations for $X_s=1.46$, (c) period 4 oscillations for $X_s=1.48$, and intermittent time traces for (d) $X_s=1.485$, (e) $X_s=2$, and (f) $X_s=4$.

of its dynamical properties. This will certainly allow for a clear insight and better understanding of the physical mechanisms responsible for the occurrence of self-pulsing in SMIB laser systems. The identification of such mechanisms has puzzled many authors [1,8,29]. Comparison of the time evolution of the atomic variables will allow for indications of the process by which self-pulsing occurs. Figure 3 represents a typical example of the atomic variable time dependence for parameter values corresponding to those of Fig. 1(a). It shows that while the field intensity [Fig. 1(a)], as well as the polarization components [Fig. 3(a)], are essentially zero between pulses, the phase between the real and the imaginary parts of the off-resonance polarization component does not remain at a fixed value, but continues to evolve in time, ultimately giving rise to the next intensity pulse. The dephasing process between the real and the imaginary parts of the atomic-polarization component seems to be the clue behind the physical mechanism of the low-excitation self-pulsing phenomena in SMIB lasers. The time evolution of the phase between p_r and p_i does not allow the dynamics of the system to come to an end, meanwhile the population-inversion variables follow the variations imposed by their own natural time rate at $1/\gamma$ [Fig. 3(b)]. This results in repetitive pulses. These facts can be fully appreciated when looking for a strategy of simplification of the 6D model. For example, if we look at the time traces of p_r and p_i we may deduce that $p_r \simeq -p_i$; this suggests that we may eliminate either equation in such a way that the variations of p_i are linked to the variations of p_r through $p_i = -wp_r$. However, replacing p_i with $-wp_r$ in the equations prevents the whole low-excitation dynamics. In short, we may conclude that self-pulsing in SMIB lasers is not to be associated with a dephasing process between the various atomic components of the different velocity groups, as suggested in Ref. [8], but rather to the complex nature of each atomic-polarization component.

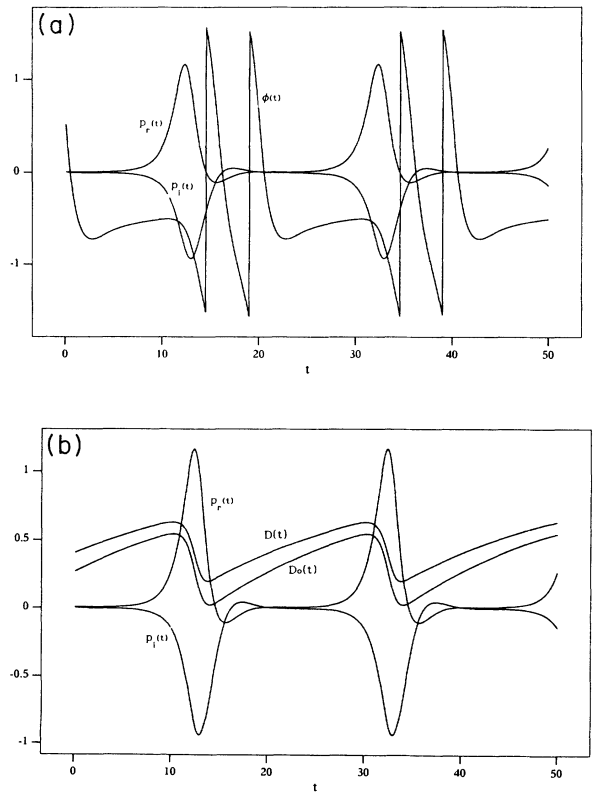

FIG. 3. Snapshots of the various interacting variables in the self-pulsing regime, for parameter values corresponding to Fig. 1.

The time evolution of D_0 and D also suggests the possibility of eliminating either equation in set (13). However, setting $D \simeq D_0$ yields another set of equations with different dynamical properties. This conclusively shows the importance of each atomic component in the 6D model. Some focus will be given to the effect of adiabatically eliminating the field variable later in the paper.

Some other interesting features which are contained in the model may be best appreciated when representing phase-space portraits in the two limiting cases of low- and high-γ values. Figure 4 shows some phase-space representations in the (E,D) plane in the case of $\gamma = 0.05$. Following an increase of the excitation parameter X_s, a series of limit cycles of increasingly doubling periodicities appear ultimately resulting in a chaotic attractor in the positive (E,D) half plane. Up to $X_s = 1.842$ the whole dynamics takes place in this half plane. A further increase of X_s results in an explosion of the chaotic attractor to the whole (E,D) plane. Beyond this X_s value the dynamical evolution takes place in the entire (E,D) plane. This behavior is physically attributed to a dramatic change (of π) in the evolving-field phase during the dynamical evolution of the system, at the point where the field variable just crosses the D axis when heading from the positive (negative) towards the negative (positive) part of the E axis. Beyond some critical value, at $X_s \simeq 2.8$, the system settles in a limit cycle in which it remains for any further increase of the excitation parameter.

The phase-space portraits for higher-γ values, $\gamma = 1$ in the case represented in Fig. 5, are suggestive of some distinctive dynamics. For low values of X_s the system describes a single-looped limit cycle in the same (E,D) half plane as in the above case. However, the first bifurcation to higher period limit cycles immediately follows the intrusion of the system onto the other half (E,D) plane. The system evolves rapidly towards a strange attractor, an example of which is shown in Fig. 5(c). In this case the attractor closely resembles the Lorenz strange attractor. The dynamics of the system remains in this strange attractor for a large range of values of the control parameter X_s contrary to the low-γ case. These apparent differences in dynamical behavior conclusively show the importance of the various decay rates which effectively control the dynamical evolution of the system.

The period-doubling sequence found in the model inspires some interest in plotting the corresponding bifurcation diagram in the case where the Feigenbaum sequence is more apparent, i.e., for $\gamma = 0.05$. Such a diagram has been numerically simulated, and is represented in Fig. 6 where the vertical axis corresponds to the

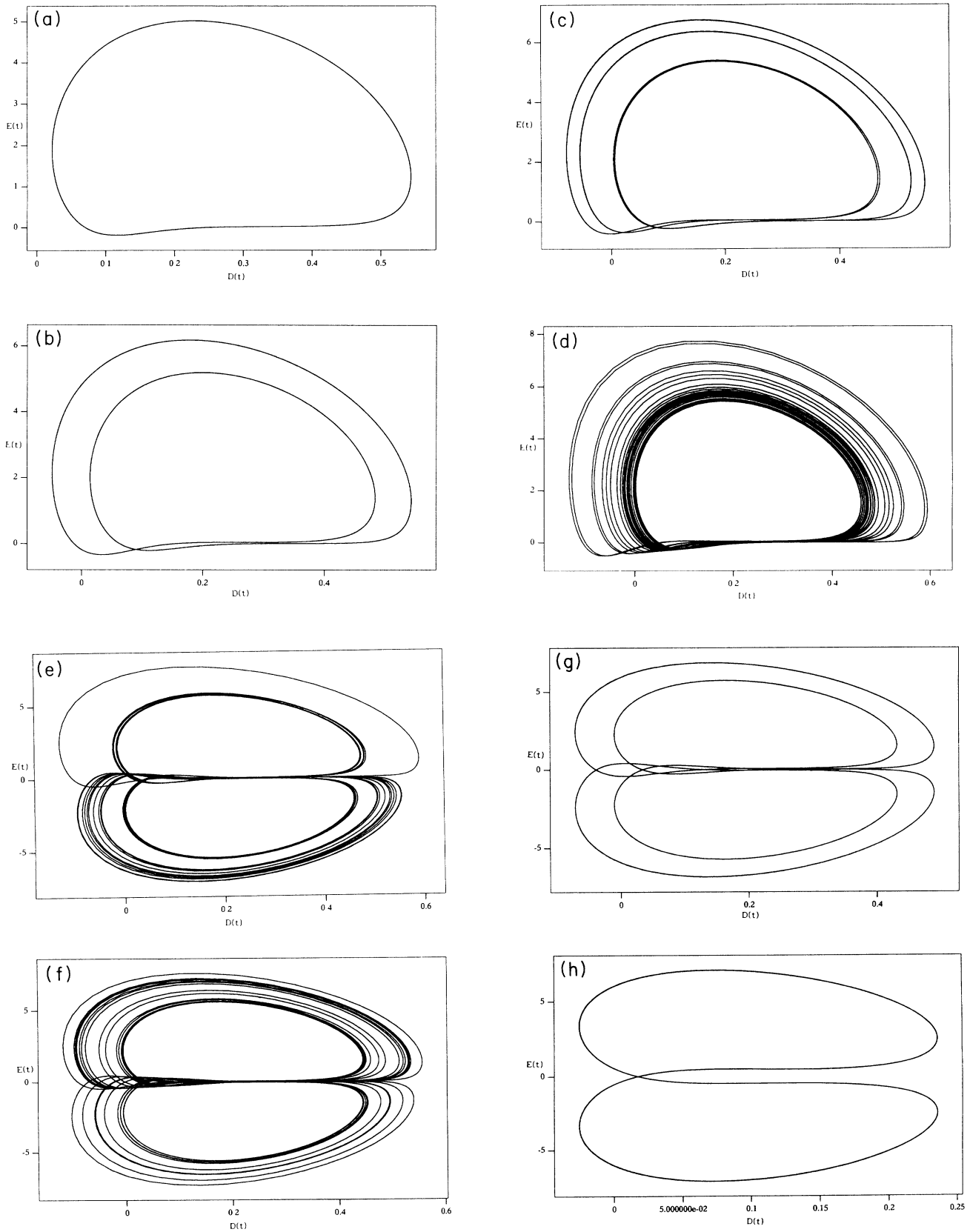

FIG. 4. Phase-space portraits in the (E,D) plane for $k=5$, $\gamma=0.05$, $w=1$, and increasing excitation parameter, showing (a) single-loop limit cycle for $X_s=1.6$, (b) double-loop limit cycle for $X_s=1.75$, and multiple-loop limit cycles culminating in an attractor: (c) $X_s=1.81$, (d) $X_s=1.842$, (e) $X_s=1.843$, (f) $X_s=1.9$. For higher-excitation levels the system is again attracted to a limit cycle: (g) $X_s=1.95$, and (h) $X_s=2.9$.

heights of the obtained pulse peaks for each scanned value of the saturation intensity X_s. Many of the above-described characteristics are clarified with the help of this diagram, which exhibits most of the properties found in the Feigenbaum period-doubling sequence *ad infinitum* with clear and distinct periodic windows. It also shows that the first branch of period doubling obtained for a low-excitation-parameter range is quite large, explaining the experimental observation of periodic double bursts in the intensity output of the high-gain He-Xe laser [24]. Also worth mentioning is the catastrophic point at $X_s \simeq 2.8$ at which the system jumps in an apparently abrupt manner from a multipeaked train of pulses to a regular and singly peaked time trace and for which the system is attracted to the limit cycle of Fig. 4(h).

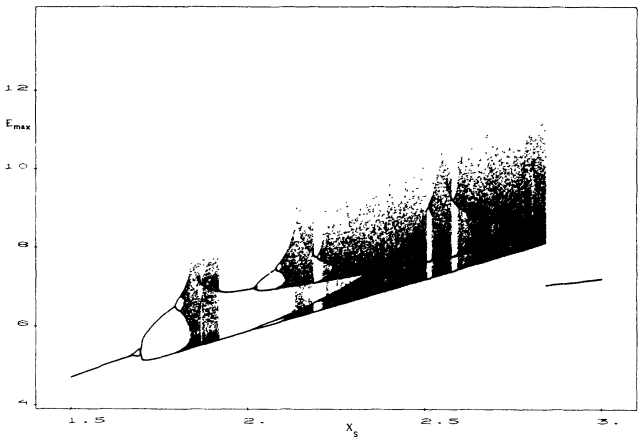

FIG. 6. Bifurcation diagram representing intensity pulse peaks with increasing X_s.

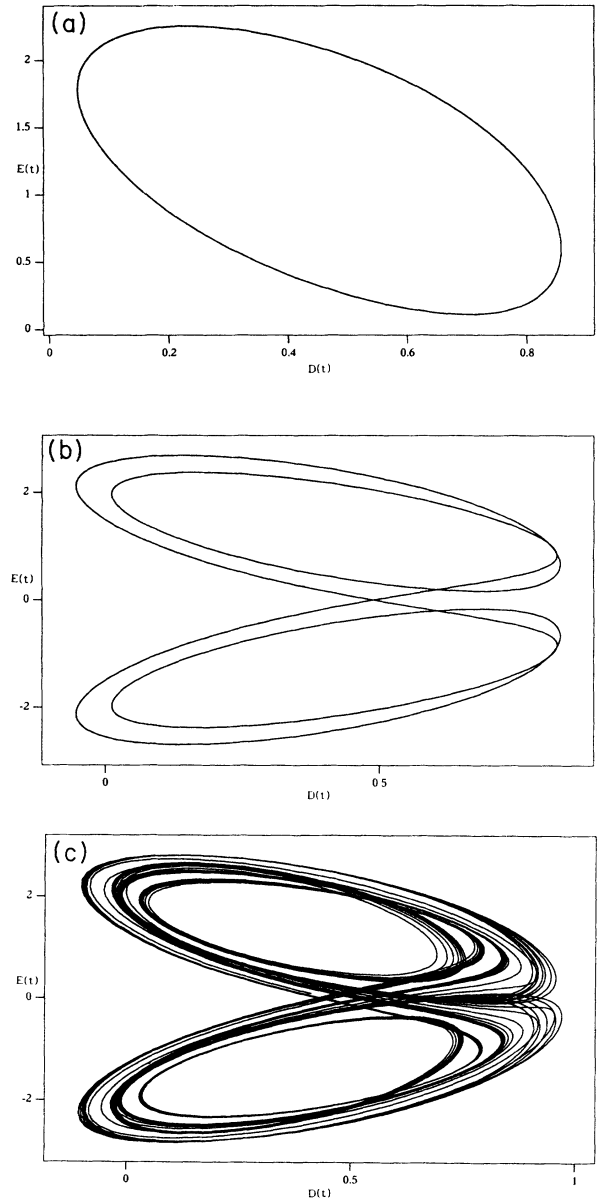

FIG. 5. Phase-space portraits in the (E,D) plane for $k=5$, $\gamma=1$, $w=2$, and (a) $X_s=1.3$, single-loop limit cycle, (b) $X_s=1.46$, double-loop limit cycle, and (c) $X_s=1.485$, a chaotic attractor in which the system settles for any further increase of X_s.

The construction of return maps may also exhibit some information that seems hidden at first sight. We have represented a few return maps, obtained by plotting successive maxima against one another, in Fig. 7. These are suggestive of the following remarks: (i) at the end of the first period-doubling sequence the return map exhibits a shape of hyperbolic form with some degree of asymmetry [Fig. 7(a)]; and (ii) the end of the second Feigenbaum sequence yields the emergence of a cusp, reminiscent of the one obtained with the Lorenz model [34], in the left part of the map. This behavior is also obtained for higher values of X_s [$X_s=2.7$ is the case represented in Fig 7(c)]. The changes in shape of the maps with increasing X_s indicate the coexistence of the Feigenbaum sequence with a Lorenz-like attractor. Coexisting attractors have already been shown to exist in lasers with injected signals [35].

The distinct dynamical properties found between the low- and the high-γ-value cases require a further analysis in connection with variations of the rate of incoherent decay of the population-inversion components and of the excitation parameter X_s. First, the evolution of the average period between pulses as a function of γ is represented in Fig. 8(a) in which the vertical axis is normalized with respect to $1/\gamma$. The plot shows an almost $1/\gamma$ dependence for which the period between pulses is quite large for small-γ values but rapidly decreases with increasing γ. In Fig. 8(b) the pulse repetition rate is also shown to increase, though in a smoother way, with increasing excitation level. The averaged pulse-intensity output also closely depends on the two parameters γ and X_s. Figure 9 shows the dependence of the averaged pulse-intensity output on the excitation parameter for various values of the incoherent decay rate. The lower plot in the figure represents the variations with X_s of the steady-state (SS) intensity that would result if the time derivatives in set (13) were all set equal to zero. Figure 9 clearly indicates that when self-pulsing sets in, each pulse

carries an averaged intensity output higher than the steady-state value, and that the averaged intensity also increases when the rate of incoherent decay of the population-inversion components decreases. These features are also contained in the integro-differential equations (1) and have already been pointed out by Casperson [23,24]. We may in addition note that the intensity carried by a single pulse increases only at the expense of pulse repetition rate in such a way that, for a given excitation level, the product γT does not appreciably vary.

Now that the dynamical properties of our model have been investigated in some detail, we shall give some attention to the influence on the behavior of the system of (a) the adiabatic elimination of the fast-relaxing field, (b) the rate-equations approximation, and (c) the addition of a detuning parameter.

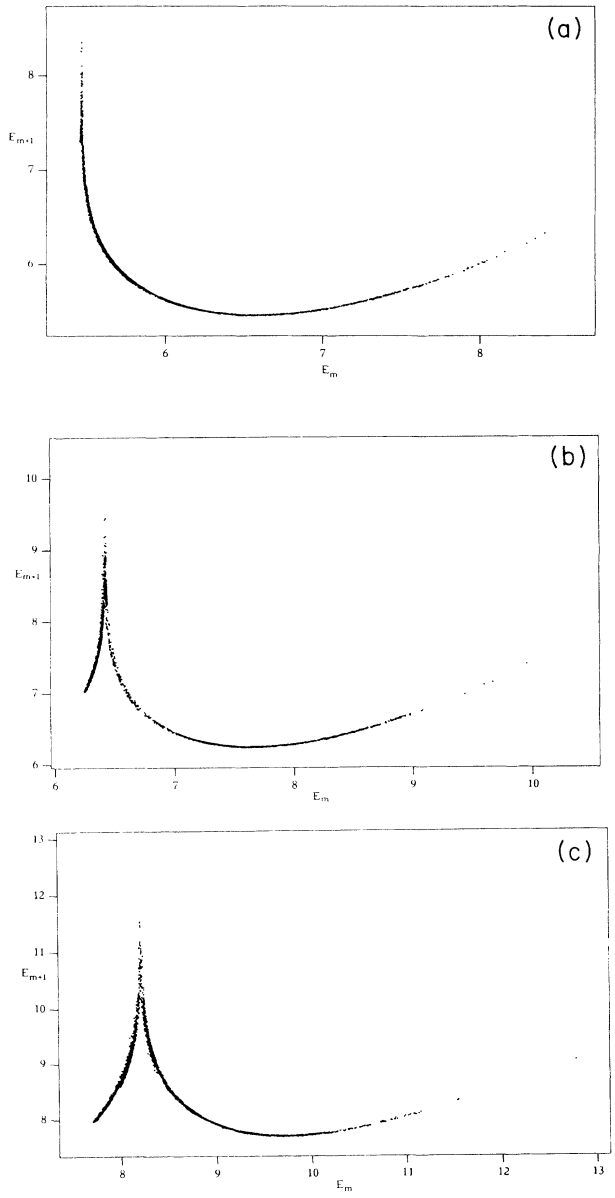

FIG. 7. Various shapes of the return maps representing successive maxima against one another in the self-pulsing regime, and for various excitation parameters (a) $X_s=1.85$ (b) $X_s=2.15$, and (c) $X_s=2.7$.

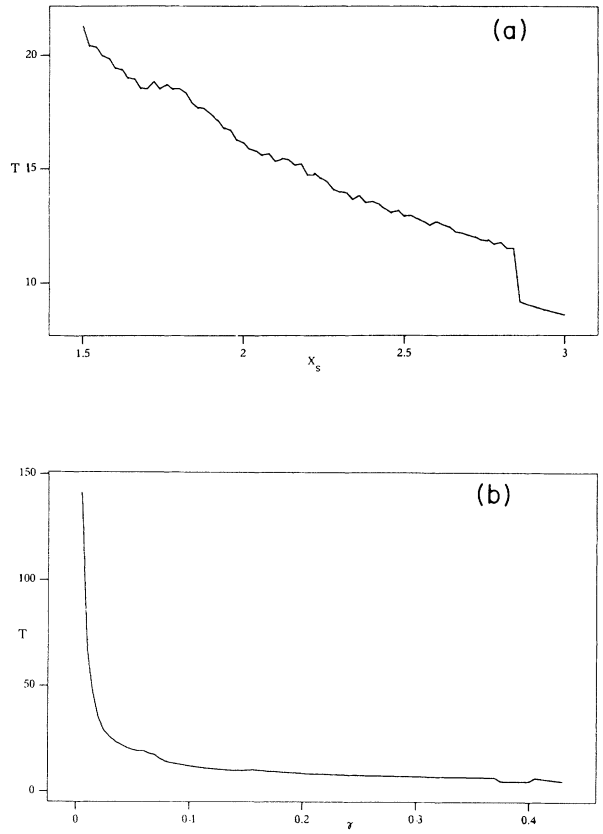

FIG. 8. Variation of the pulsation period, (a) as a function of X_s, for $\gamma=0.05$, and (b) as a function of γ, for $X_s=1.5$.

A. Adiabatic-field approximation

Adiabatically eliminating the field variable from set (13) yields a 5D model in which the output field intensity

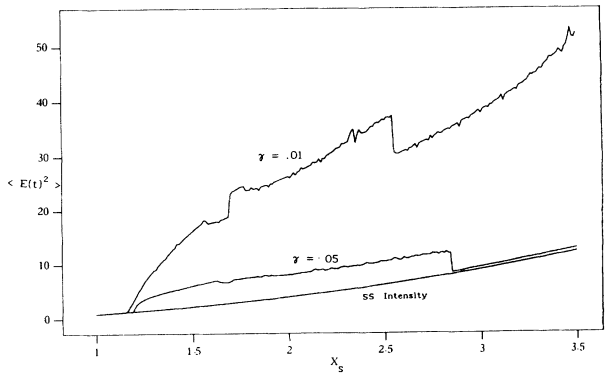

FIG. 9. Average output intensity for various γ values, with increasing X_s. The lower plot represents the value of the intensity variable when the field derivatives in Eqs. (6) are all set equal to zero.

instantaneously follows the variations of the atomic-polarization components p_r and p_0, whose dynamical evolution are in turn closely dependent on their exact interaction with the population-inversion components:

$$\frac{d(p_r)}{dt} = -p_r + wp_i - 2C(2p_r + p_0)D(t) , \tag{16a}$$

$$\frac{d(p_i)}{dt} = -p_i - wp_r , \tag{16b}$$

$$\frac{d(p_0)}{dt} = -p_0 - 2C(2p_r + p_0)D_0(t) , \tag{16c}$$

$$\frac{d[D(t)]}{dt} = -\gamma[D(t) + 1 - 2C(2p_r + p_0)p_r] , \tag{16d}$$

$$\frac{d[D_0(t)]}{dt} = -\gamma[D_0(t) + 1 - 2C(2p_r + p_0)p_0] , \tag{16e}$$

and $E(t)$ variations are deduced from

$$E(t) = -2C[2p_r(t) + p_0(t)] . \tag{17}$$

The numerical analysis of this new set has been undertaken for the same range of parameter values as in the above cases. This will allow for straightforward conclusions on the effect brought to the dynamical aspects from the

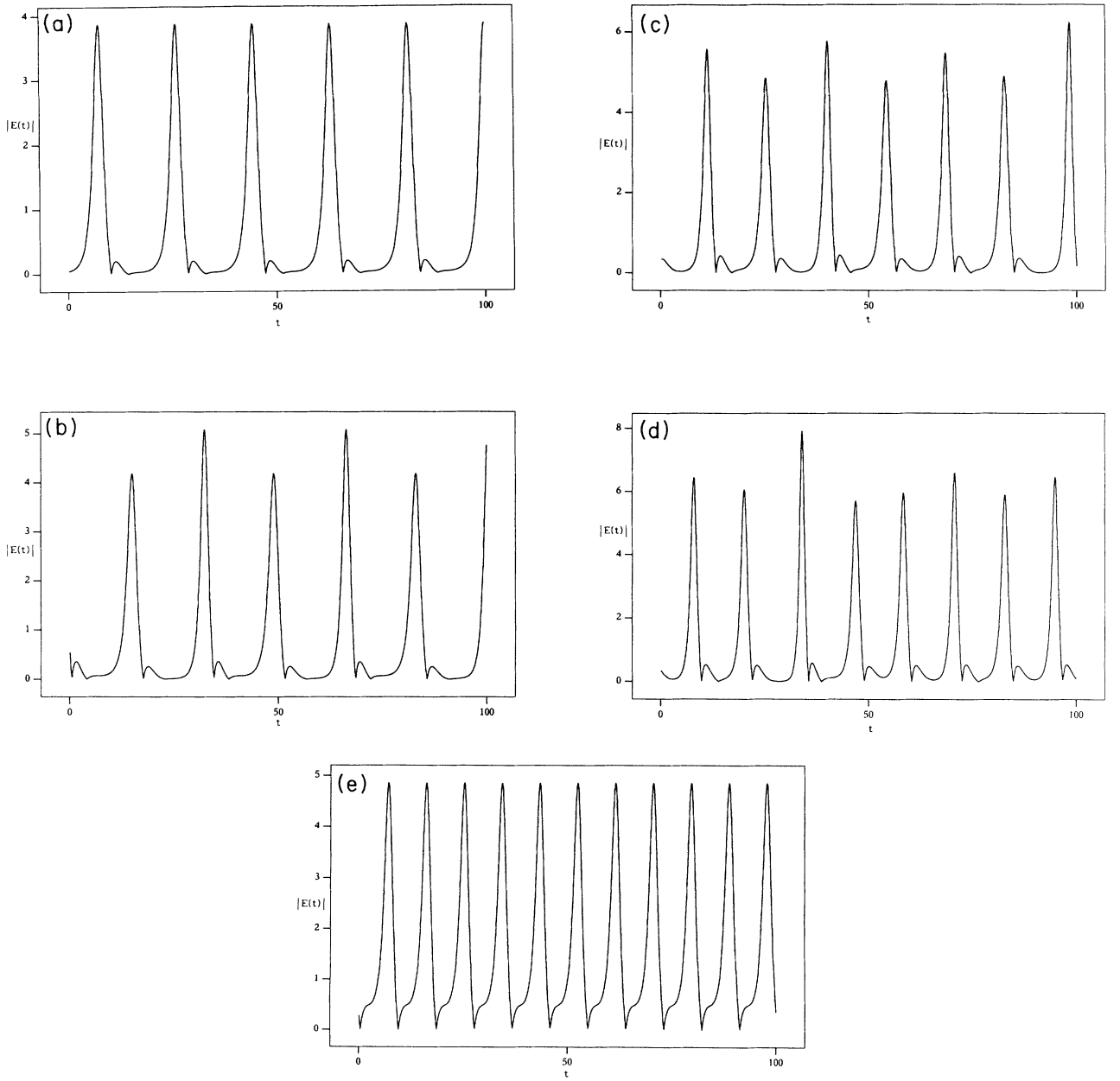

FIG. 10. Intensity pulse trains obtained in the adiabatic-field approximation, for $\gamma = 0.05$, and (a) $X_s = 1.3$, (b) $X_s = 1.5$, (c) $X_s = 1.75$, (d) $X_s = 2.1$, and (e) $X_s = 2.2$.

neglect of the field derivative. Results of a few typical scans are represented in Figs. 10 and 11. It is evident from these figures that little effect is brought about by the adiabatic elimination of the fast field variable. The deep qualitative nature of the dynamics has not been altered whatsoever. The system exhibits the whole properties of the 6D model, apart from the fact that the hierarchy of the different bifurcations has undergone a small shift to lower values of the excitation parameter. For example, the first period-doubling bifurcation occurs at $X_s \simeq 1.7$ for the 6D model, whereas it takes place at $X_s \simeq 1.4$ in the 5D case for $\gamma = 0.05$. From $X_s \cong 0.7$ to 1.4, the output consists of reproducible and regular pulse trains. Bifurcations to higher-order periodicities start at $X_s \cong 1.4$ to end at $X_s \cong 2.1$. At $X_s \cong 2.2$, and up, the time trace consists again of periodic and stable intensity pulses with increasing repetition rate with increasing X_s. The same qualitative changes are also seen for $\gamma = 1$ for low-excitation values. In this case irregular solutions are only found in the range $0.9 < X_s < 1.1$ with a double-period window for $1.1 < X_s < 1.2$. At $X_s \cong 1.3$, and up, the system stabilizes again to a regular oscillating intensity output; this is to be compared with the results exhibited by the 6D model for which the system showed a persistent chaotic output for high-excitation levels. We conclude that the effect of adiabatically eliminating the field vari-

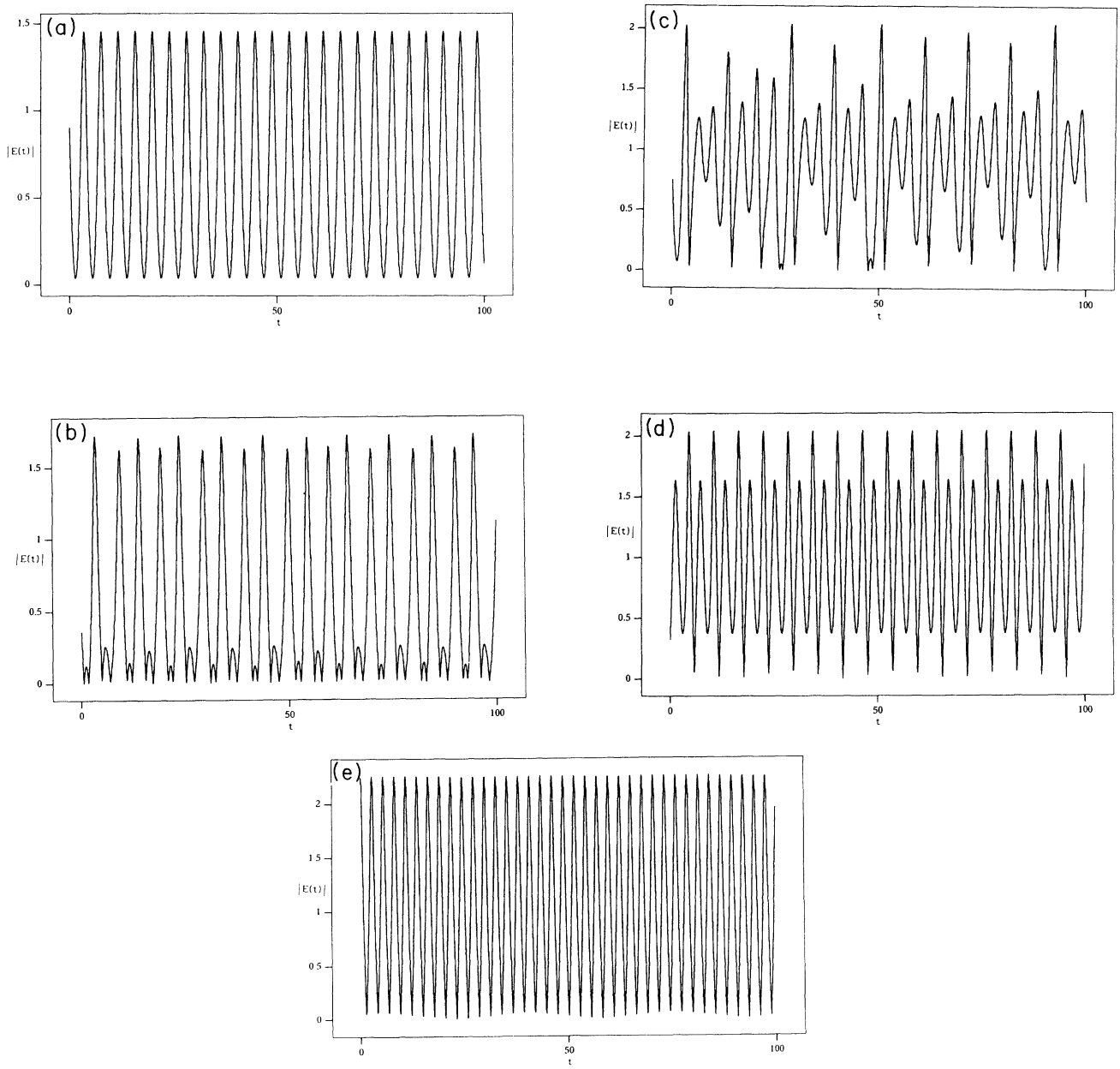

FIG. 11. Intensity time traces for $\gamma = 1$ in the adiabatic-field limit for (a) $X_s = 0.8$, (b) $X_s = 0.9$, (c) $X_s = 1$, (d) $X_s = 1.1$, (e) $X_s = 1.3$.

able in SMIB lasers has no definite influence for low-excitation levels, especially for small-γ values. However, for high-excitation parameters, the dynamical properties, which were shown to be close to the ones exhibited by the Lorenz model of turbulence in fluids in the 6D case, completely disappear for high-excitation and high-γ values. This last case seems to indicate that the field variable has some non-negligible influence on the dynamical properties of the system. This fact is quite understandable in view of the fact that in this case the value of γ is of the same order of magnitude as k, so that it is not correct to neglect the field derivative, contrary to the case of small γ where this approximation is justified.

We also note the decreased value of the second intensity threshold; while, for example, $X_{\text{sth}} \simeq 1.1$ for the 6D case it is only $X_{\text{sth}} \simeq 0.7$ for the 5D model. It is seen that, for $\gamma = 0.05$, the dynamical evolution has much the same qualitative features as the 6D case in the whole range of X_s values. This leads to the following remark: The role of the field as a dynamical variable is not of relevance, at least for the qualitative features, in the physical mechanism behind self-pulsing in SMIB laser systems. This also explains the fact that a bad-cavity configuration is required to obtain self-pulses; it allows the dynamical variables p_r, p_i, and D to freely interact, yielding intensity pulses at maximum coherence between these variables. In the case of a good cavity the field variable would be so intense that it would destroy the effect of the free interaction between p_r, p_i, and D; E would then be the only order parameter thus preventing any deviation from steady state.

B. Rate-equations approximation

The rate-equations approximation only holds when the medium is supposed to respond instantaneously to the field inside the cavity (we may recall that the remarkable work of Lamb on laser theory [27] is completely based on these assumptions). The obtained equations stem from the neglect of the variations of the atomic-polarization components. When this is done we are left with a set of three equations:

$$\frac{d[E(t)]}{dt} = -k\left[E(t)+2C\left[\frac{2}{(1+w^2)}D(t) + D_0(t)\right]E(t)\right], \tag{18a}$$

$$\frac{d[D(t)]}{dt} = -\gamma\left[1+\left[1+\frac{[E(t)]^2}{(1+w^2)}\right]D(t)\right], \tag{18b}$$

$$\frac{d[D_0(t)]}{dt} = -\gamma(1+\{1+[E(t)]^2\}D_0(t)) . \tag{18c}$$

The numerical solutions of these equations, which are equivalent to the well-known rate equations, yield a dynamically stable output for any chosen range of values of the various parameters. This again demonstrates the relevance of the atomic-polarization components in SMIB laser dynamics.

C. Effect of detuning

Detuning the laser from the atomic-line center greatly influences the dynamical properties of laser systems. This also has been a subject that received considerable attention [36–39]. It is found that the dynamics of the system is very much altered even with very small amounts of detunings. Some authors have also reported a stabilizing effect [36] on the output intensity when a laser is detuned from its line center. However, the addition of a detuning parameter takes the system over a higher degree of complexity. Our 6D model expands to an 11D set of equations with the inclusion of detuning. In the 3D case of SMHB lasers five equations are necessary when detuning is included [37]. The simplicity of the system is quickly lost. The set of equations which accurately describes detuning effects takes the form

$$\frac{d[E(t)]}{dt} = -k\left[(1+i\Delta_{\text{CL}}/k)E(t) + 2C\sum_{n=-1}^{+1} p(w_n,t)\right], \tag{19a}$$

$$\frac{d[p(w_n,t)]}{dt} = -[1+i(w_n+\Delta_{\text{AL}})]p(w_n,t) + E(t)D(w_n,t) , \tag{19b}$$

$$\frac{d[D(w_n,t)]}{dt} = -\gamma\{\tfrac{1}{2}[E(t)p^*(w_n,t)+E^*(t)p(w_n,t)] + D(w_n,t)+1\} , \quad n=-1,0,+1 \tag{19c}$$

where Δ_{CL} is the laser-cavity frequency offset, and Δ_{AL} the laser-atomic-line detuning parameter, both scaled to the polarization relaxation rate.

For a rigorous analysis of detuning effects, one has to extract, for a given value of the atomic-cavity detuning Δ_{AL}, the laser field frequency offset from line center, as given by the steady-state complex equations for the laser operating intensity and dispersion relation for the frequency: Δ_{AL} must satisfy, with X_s, the steady-state equations derived from the above set as

$$2C\sum_{n=-1}^{+1}\frac{1}{1+(\Delta_{\text{AL}}+w_n)^2+X_s^2} = 1 , \tag{20a}$$

$$2C\sum_{n=1}^{+1}\frac{w_n+\Delta_{\text{AL}}}{1+(\Delta_{\text{AL}}+w_n)^2+X_s^2} = \frac{\Delta_{\text{LC}}}{k} . \tag{20b}$$

However, we found that deviations of the detuning parameter from its value as given by the state equation do not significantly alter the qualitative behavior which will allow one to draw the correct conclusions pertaining to the effect of a detuning parameter on the general dynamical features of the system. For this reason, it is not of absolute necessity to stick to the values of Δ_{AL} and Δ_{LC} given by the state equation. For simplicity, the detuning parameter is scanned independently of the state equation in our numerical calculations. Also, for a good range of X_s values we have found that Δ_{AC} does not appreciably

deviate from Δ_{AL}, so that in the analysis a single parameter is used instead of Δ_{AC} and Δ_{AL}.

As in the above case, we shall separate the study between the high- and the low-γ values. Although the same general evolution has been found for smaller values of Δ_{AC}, we shall limit our description to the case $\Delta_{AC}=\Delta_{LC}=0.1$ (recall, however, that Δ_{AC} is also a normalized quantity with respect to the polarization relaxation rate).

From large scans of the excitation parameter, the following general features are recognized: For $\gamma=0.05$, the low-excitation period-doubling sequence *ad infinitum* of Fig. 1 disappears in favor of a regular train of pulses up to $X_s=-2$, at which point the second period-doubling sequence starts. The variations between pulse peaks are, however, smaller as opposed to the case without detuning. At $X_s=2.7$, the output again consists of periodic and regularly spaced pulses; for $\gamma=1$, the stabilizing effect is much more enhanced for low values of X_s; up to $X_s=1.5$ the whole structure of the chaotic dynamics via a small period-doubling window (found in the 6D case) disappears in favor of a stable periodic oscillation which gives birth to a period-doubling sequence in a rather large window as opposed to the 6D case, especially the first

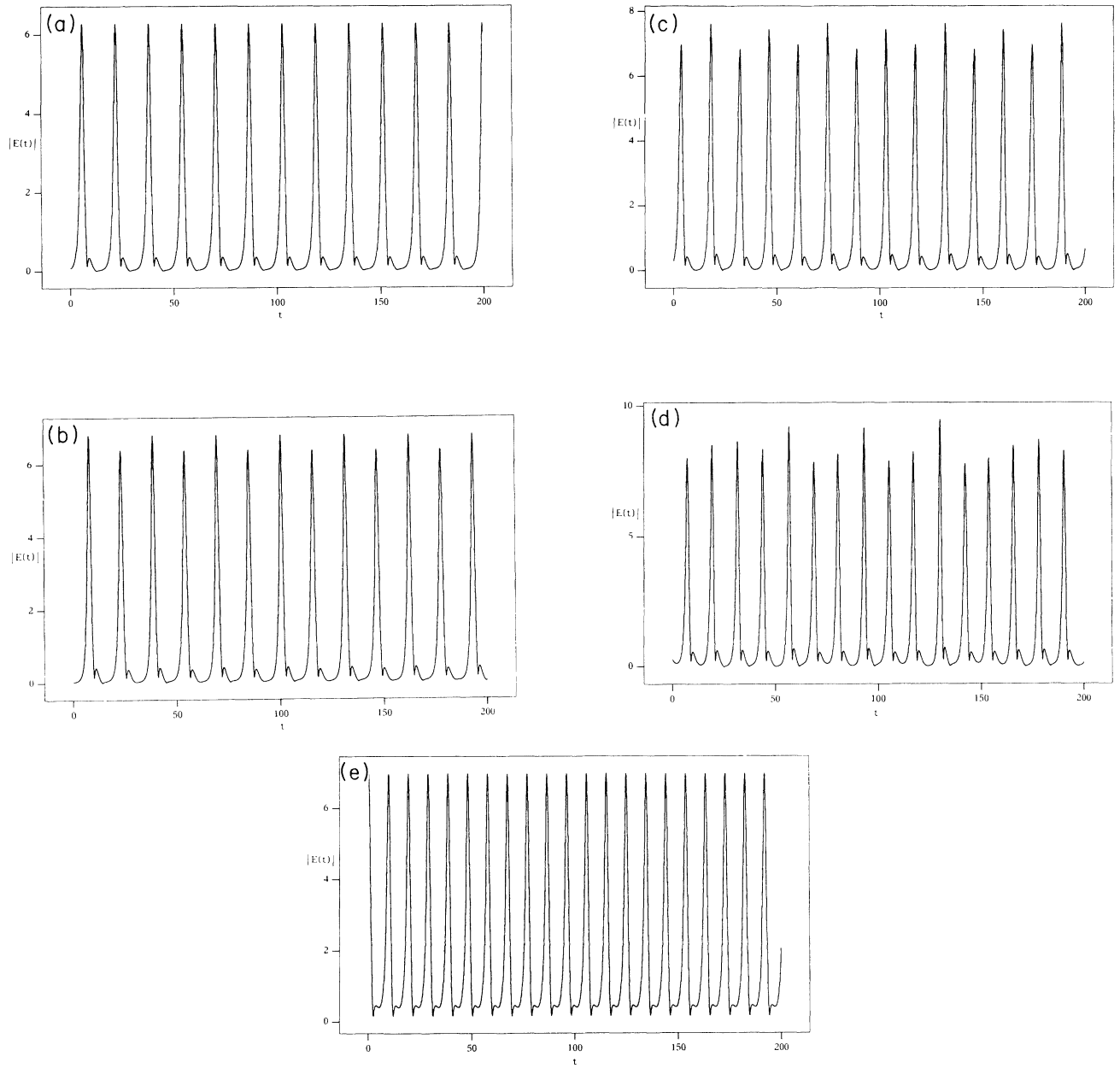

FIG. 12. Effect of a detuning parameter $\Delta=0.1$ on the intensity time traces of Fig. 1 (a) $X_s=2$, (b) $X_s=2.1$, (c) $X_s=2.3$, (d) $X_s=2.7$, and (e) $X_s=2.8$.

period-doubled oscillation which starts at $X_s=1.6$ and persists up to $X_s=2$. A further increase of the control parameter yields a chaotic output with smaller peak-to-peak variations. (See Figs. 12 and 13.)

The following conclusions may be drawn from these observations. Despite the fact that the additional detuning parameter takes the system to a phase space of higher dimensionality, its evolution in this space undergoes a much less unstable dynamics with respect to the 6D case. This conclusively demonstrates that the dynamical complexity of a system does not necessarily increase with its phase-space dimension but rather depends on the exact form of the interacting variables of the system.

We also bring attention to the fact that, up to now, the whole description of the system's dynamics has been represented in terms of the intensity output, which represents the experimentally accessible variable. However, we may have chosen the study in terms of other variables such as the real or the imaginary part of the field, an example of which is represented in Fig. 14. It clearly appears that the field's real and imaginary parts follow distinct evolutions which may lead to spurious conclusions if the system's dynamics were studied in terms of these variables. Some care has to be taken con-

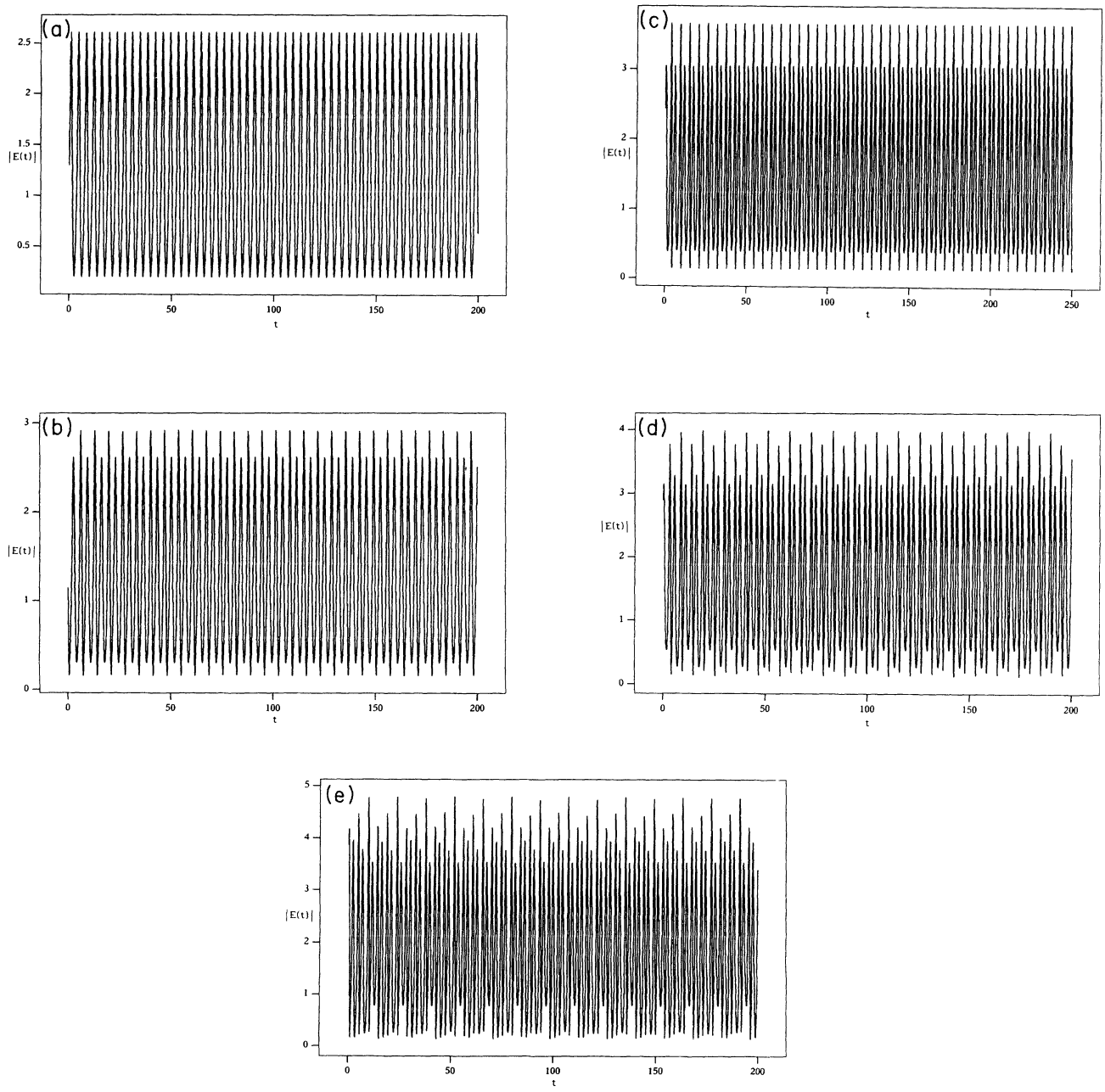

FIG. 13. Effect of the same detuning parameter ($\Delta=0.1$) on the intensity time traces of Fig. 2 for (a) $X_s=1.5$, (b) $X_s=1.6$, (c) $X_s=1.9$, (d) $X_s=2$, and (e) $X_s=2.3$.

cerning the correct choice in order to avoid spurious conclusions stemming from physically meaningless variables. In our case the real and imaginary parts of the field are simply related through a phase term $\phi(t)$, so that the relations

$$E_r(t)=E(t)\cos[\phi(t)],\quad E_i(t)=E(t)\sin[\phi(t)]\ , \tag{21a}$$

and

$$E(t)^2=E_r(t)^2+E_i(t)^2 \tag{21b}$$

yield an evolution for the real and the imaginary parts through $\phi(t)$ which modulates their temporal traces. Such an evolution does not effect the field itself. These facts may be best appreciated when projecting the dynamics to phase planes: in the (E_r,D) or (E_i,D) plane [Fig. 15(a)], the system describes an apparently multiloop limit cycle or even a chaotic attractor, while in the (E_r,E_i) plane [Fig. 18(b)] the dynamics takes place in diagrams reminiscent of margueurites with petals of different lengths depending on the state of the system; in the $([E],D)$ plane [Fig. 15(c)] this whole process takes place in a double-looped limit cycle which yields the correct double pulses in the intensity output.

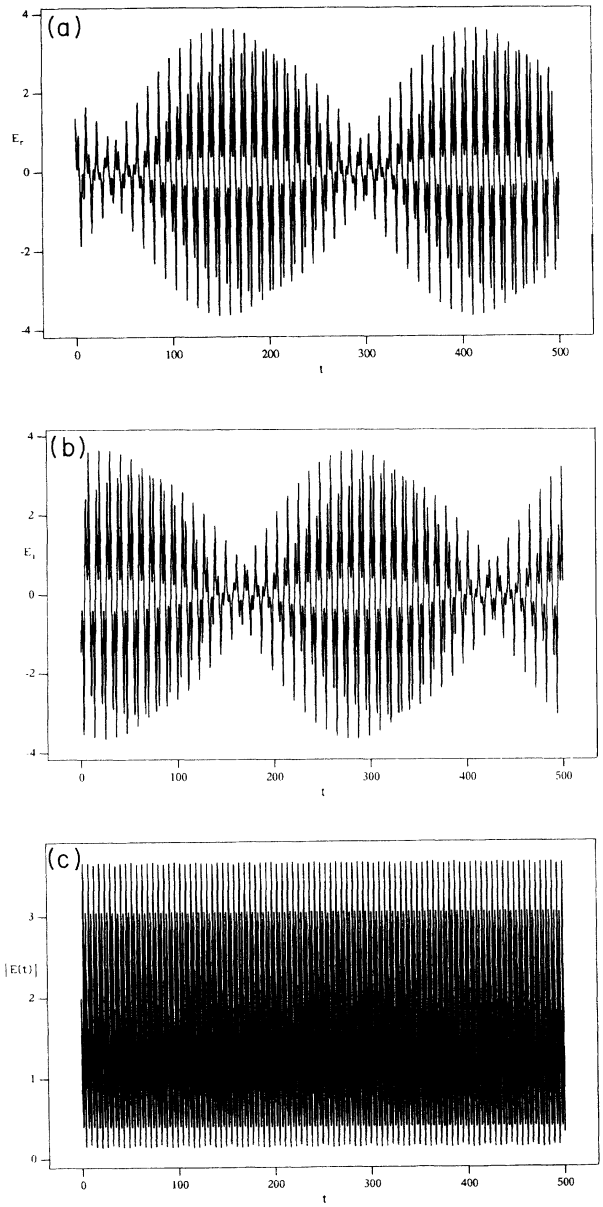

FIG. 14. Comparison between the time evolution of (a) the real part, (b) the imaginary part, and (c) the modulus of the output field, for parameters $X_s=1.0$, $\gamma=1$, $w=2$, and $\Delta=0.1$.

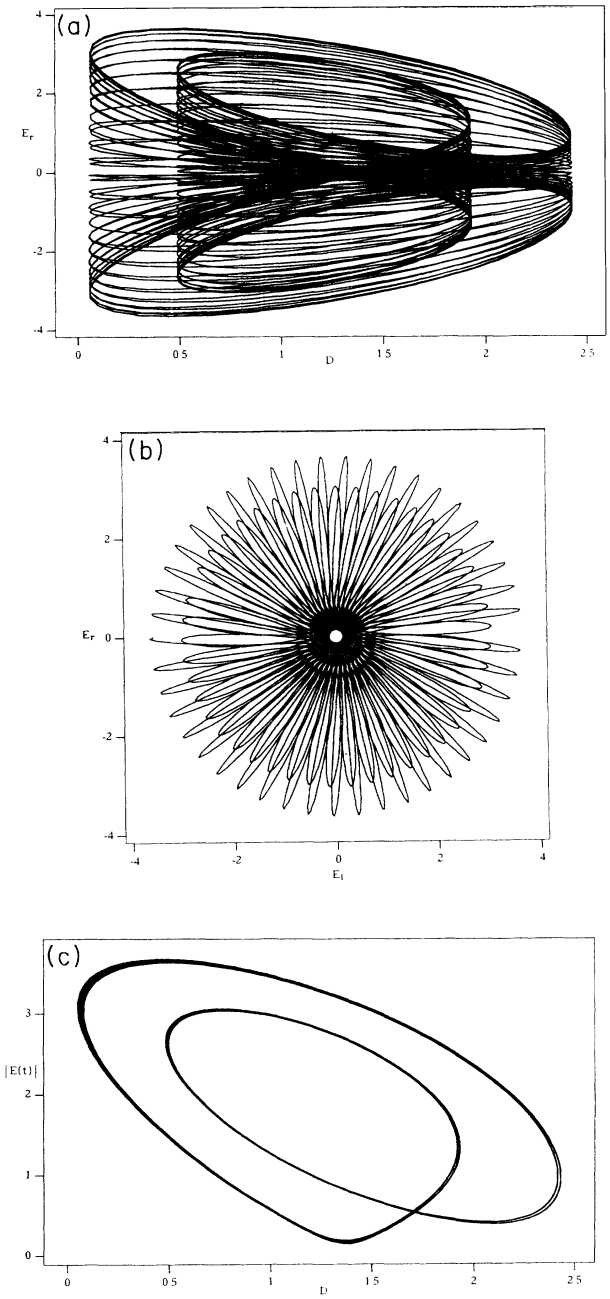

FIG. 15. Phase-space representations in (a) the (E_r,D) plane, (b) the (E_r,E_i) plane, and (c) the (E,D) plane for the same parameter values as in Fig. 14.

V. CONCLUSION

We have presented a review of a few low-dimensional models describing some of the dynamical properties of the single-mode inhomogeneously broadened, unidirectional ring laser. Each of these models has been analyzed and its limits pointed out in the frame of the system's control parameters. A 6D model which contains most of the dynamical aspects of the integro-differential Maxwell-Bloch equations has been constructed. A first numerical analysis of our model, for parameter values corresponding to some experimental investigations on the far-infrared laser, and on the He-Xe laser, shows a fairly good account of the reported dynamics of these systems. A deep investigation has yielded the recognition of some physical processes responsible for the dynamical properties of SMIB lasers. The analysis has, deliberately, been limited to experimentally accessible parameters. The survey insisted more on qualitative description. Since the first aim of this paper was the construction of low-dimensional models exhibiting dynamical aspects reminiscent of the infinite-dimensional integro-differential Maxwell-Bloch equations, exact quantitative correspondence is necessarily left out. Nevertheless we have shown that qualitative description of SMIB laser dynamics is possible with low-dimensional models, which, beyond their simpler numerical handling, allow for simpler understanding of the physics behind the wealth of dynamical behavior inherent in SMIB laser systems.

ACKNOWLEDGMENT

It is a great pleasure to acknowledge permanent support and help from Professor G. Stephan.

*Permanent address: USTHB, Institut de Physique, Laboratoire Lasers, BP 32, El-Alia Bab-Ezzouar, Algiers, Algeria.

[1] L. W. Casperson and A. Yariv, IEEE J. Quantum Electron. **QE-8**, 69 (1972).
[2] L. W. Casperson, in *Laser Physics,* edited by J. Harvey and D. F. Walls, Lecture Notes in Physics Vol. 182 (Springer-Verlag, Berlin, 1983), p. 88.
[3] N. B. Abraham, T. Chyba, M Coleman, R. S. Gioggia, N. J. Halas, S. N. Liu, M. Maeda, and J. C. Wesson, in Ref. [2], p. 107.
[4] M. Maeda and N. B. Abraham, Phys. Rev. A **26**, 3395 (1982).
[5] R. S. Gioggia and N. B. Abraham, Phys. Rev. Lett. **51**, 650 (1983); Opt. Commun. **47**, 278 (1983); Phys. Rev. A **29**, 1304 (1984).
[6] J. Bentley and N. B. Abraham, Opt. Commun. **41**, 52 (1982).
[7] N. B. Abraham, L. A. Lugiato, P. Mandel, L. M. Narducci, and D. K. Bandy, J. Opt. Soc. Am. B **2**, 5 (1985).
[8] D. K. Bandy, L. M. Narducci, L. A. Lugiato, and N. B. Abraham, J. Opt. Soc. Am. B **2**, 56 (1985).
[9] P. Mandel, J. Opt. Soc. Am B **2**, 112 (1985).
[10] Ji-yue Zhang, H. Haken, H. Ohno, J. Opt. Soc. Am. B **2**, 141 (1985).
[11] S. Hendow and M. Sargent, J. Opt. Soc. Am. B **2**, 84 (1985).
[12] M. L. Shih, P. W. Milonni, and J. R. Ackerhalt, J. Opt. Soc. Am. B **2**, 130 (1985).
[13] M. Minden and L. W. Casperson, J. Opt. Soc. Am. B **2**, 120 (1985).
[14] M. F. H. Tarroja, N. B. Abraham, D. K. Bandy, and L. M. Narducci, Phys. Rev. A **34**, 3148 (1986).
[15] A. Gurtovnic, Izv. Vyss. Uchebn. Zaved. Radiofiz. **1**, 83 (1958).
[16] E. R. Buley and F. W. Cummings, Phys. Rev. **134**, A1454 (1964).
[17] H. Haken, Phys. Lett. **A53**, 77 (1975).
[18] E. N. Lorenz, J. Atmos. Sci. **20**, 130 (1963).
[19] P. Berge, Y. Pomeau, and C. Vidal, *L'Ordre dans le Chaos: vers une Approche Deterministe de la Turbulence* (Hermann, Paris, 1985).
[20] *Universality in Chaos,* edited by P. Cvitanovich (Hilger, Bristol, 1984).
[21] H. G. Schuster, *Deterministic Chaos* (VCH, Weinheim, 1988).
[22] A. Yariv, *Quantum Electronics,* 2nd ed. (Wiley, New York, 1975), p. 277.
[23] L. W. Casperson, IEEE J. Quantum Electron. **QE-14**, 756 (1978).
[24] L. W. Casperson, Phys. Rev. A **21**, 911 (1980).
[25] L. W. Casperson, J. Opt. Soc. Am. B **2**, 62 (1985); **2**, 73 (1985).
[26] M. Sargent III, M. O. Scully, and W. E. Lamb, Jr., *Laser Physics* (Addison-Wesley, Reading, MA, 1974).
[27] W. E. Lamb, Jr., Phys. Rev. **134**, A1429 (1964).
[28] R. Graham and Y. Cho, Opt. Commun. **47**, 52 (1983).
[29] B. Meziane, Opt. Commun. **75**, 287 (1990).
[30] B. Meziane, *OSA Proceedings on Nonlinear Dynamics in Optical Systems,* edited by N. B. Abraham, E. Garmire, and P. Mandel (Optical Society of America, Washington, DC, 1991), Vol. 7, p. 519.
[31] U. S. Idiatulin and A. V. Uspenskii, Radiotech. Electron. **18**, 580 (1973); [Radio Eng. Electron. Phys. (USSR) **18**, 422 (1973)].
[32] N. B. Abraham, D. Dangoisse, P. Glorieux, and P. Mandel, J. Opt. Soc. Am. B **2**, 23 (1985).
[33] H. Haken, *Synergetics: An Introduction,* 3rd ed. (Springer-Verlag, Berlin, 1983); *Advanced Synergetics* (Springer-Verlag, Berlin, 1983).
[34] C. Sparrow, *The Lorenz Equations: Bifurcations, Chaos and Strange Attractors,* Applied Mathematical Sciences, Vol. 41 (Springer-Verlag, Heidelberg, 1982).
[35] D. K. Bandy, L. M. Narducci, L. A. Lugiato, J. Opt. Soc. Am. B **2**, 148 (1985).
[36] H. Zeghlache and P. Mandel, J. Opt. Soc. Am. B **2**, 18 (1985).
[37] P. Mandel and H. Zeghlache, Opt. Commun. **47**, 146 (1983).
[38] K. Otsuka and H. Kawaguchi, Phys. Rev. A **29**, 2953 (1984).
[39] K. Otsuka and H. Kawaguchi, Phys. Rev. A **30**, 1576 (1984).

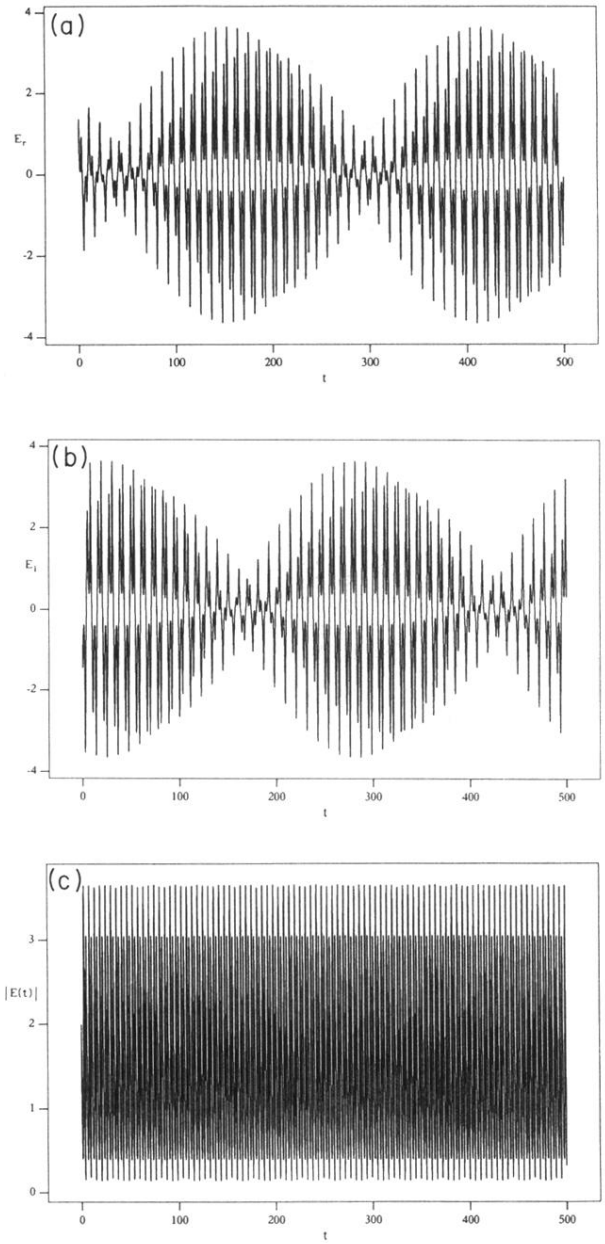

FIG. 14. Comparison between the time evolution of (a) the real part, (b) the imaginary part, and (c) the modulus of the output field, for parameters $X_s = 1.0$, $\gamma = 1$, $w = 2$, and $\Delta = 0.1$.

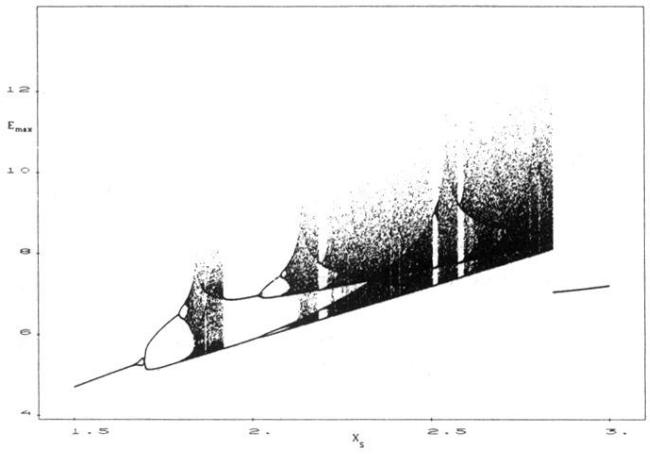

FIG. 6. Bifurcation diagram representing intensity pulse peaks with increasing X_s.